

Long time position distribution of an active Brownian particle in two dimensions

Urna Basu,¹ Satya N. Majumdar,² Alberto Rosso,² and Grégory Schehr²

¹Raman Research Institute, Bengaluru 560080, India

²LPTMS, CNRS, Univ. Paris-Sud, Université Paris-Saclay, 91405 Orsay, France

We study the late time dynamics of a single active Brownian particle in two dimensions with speed v_0 and rotation diffusion constant D_R . We show that at late times $t \gg D_R^{-1}$, while the position probability distribution $P(x, y, t)$ in the x - y plane approaches a Gaussian form near its peak describing the typical diffusive fluctuations, it has non-Gaussian tails describing atypical rare fluctuations when $\sqrt{x^2 + y^2} \sim v_0 t$. In this regime, the distribution admits a large deviation form, $P(x, y, t) \sim \exp[-t D_R \Phi(\sqrt{x^2 + y^2}/(v_0 t))]$, where we compute the rate function $\Phi(z)$ analytically and also numerically using an importance sampling method. We show that the rate function $\Phi(z)$, encoding the rare fluctuations, still carries the trace of activity even at late times. Another way of detecting activity at late times is to subject the active particle to an external harmonic potential. In this case we show that the stationary distribution $P_{\text{stat}}(x, y)$ depends explicitly on the activity parameter D_R^{-1} and undergoes a crossover, as D_R increases, from a ring shape in the strongly active limit ($D_R \rightarrow 0$) to a Gaussian shape in the strongly passive limit ($D_R \rightarrow \infty$).

PACS numbers: 05.70.Ln 05.40.-a 83.10.Pp

I. INTRODUCTION

Recent years have seen enormous activities, both theoretical and experimental, in the study of the dynamics of self-propelled active particles. These self-propelled particles generate dissipative directed motion by consuming energy directly from the environment [1–5] and appear in a wide variety of biological and soft matter systems which include bacterial motion [6, 7], cellular tissue behaviour [8], formation of fish schools [9, 10] as well as granular matter [11, 12] and colloidal surfers [13], amongst others. For interacting self-propelled particles novel collective behaviours have been observed such as flocking [14, 15], clustering [13, 16–18], phase separation [19–21] and absence of well defined pressure [22]. Interestingly, even in the absence of interactions, the spatio-temporal dynamics of a *single* self-propelled particle exhibits rich and complex behaviour. This has led to a flurry of recent activities on the study of the stochastic processes describing the motion of a single self-propelled particle [3, 23–46].

Among various models of a single self-propelled particle, perhaps one of the simplest is the so called active Brownian particle (ABP) in two dimensions. An ABP is a single overdamped particle which moves in the $2d$ x - y plane with a constant speed v_0 . In addition to its Cartesian coordinates, $(x(t), y(t))$, the particle also carries an internal “spin” given by the orientational angle $\phi(t)$ of its velocity (see Fig. 1). This internal degree of freedom $\phi(t)$ generates the self-propulsion. The three coordinates $x(t)$, $y(t)$, and $\phi(t)$ evolve with time via the coupled Langevin equations [3–5]

$$\begin{aligned} \dot{x} &= v_0 \cos \phi(t) \\ \dot{y} &= v_0 \sin \phi(t) \\ \dot{\phi} &= \sqrt{2D_R} \eta_\phi(t). \end{aligned} \quad (1)$$

Here $\eta_\phi(t)$ is a Gaussian white noise with zero mean and a correlator $\langle \eta_\phi(t) \eta_\phi(t') \rangle = \delta(t - t')$. Thus, the ori-

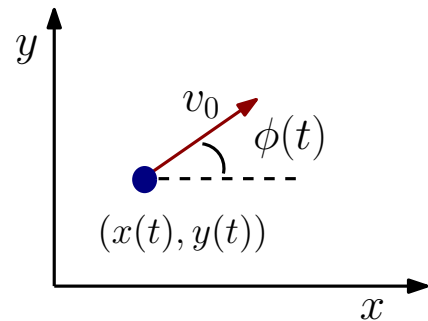


FIG. 1. An active Brownian particle at time t moving in the x - y plane with velocity v_0 . The internal degree of freedom $\phi(t)$ corresponds to the orientational angle of its velocity.

entational angle $\phi(t)$ undergoes rotational diffusion with a diffusion constant D_R . In principle one can also consider an additive translational white noise with diffusion constant D_T in both x and y equations. However it turns out that this additive noise does not qualitatively change the physics of the problem. Hence, for simplicity we drop it in the rest of the paper by setting $D_T = 0$.

The angle $\phi(t)$ is just a standard one dimensional Brownian motion with auto-correlation $\langle \phi(t_1) \phi(t_2) \rangle = 2D_R \min\{t_1, t_2\}$. Note that here the x and y coordinates are coupled through the angle $\phi(t)$ and hence are correlated. This is the origin of “activity” in the model. This is different from the standard “passive” Brownian particle (PBP) where the two coordinates evolve independently as $\dot{x} = \sqrt{2D} \eta_x(t)$ and $\dot{y} = \sqrt{2D} \eta_y(t)$, where $\eta_{x,y}(t)$ are independent delta correlated white noises with zero mean, and D is the standard diffusion constant. Indeed, Eq. (1) can be expressed in the same form as that of a PBP by writing $\dot{x} = \xi_x(t)$ and $\dot{y} = \xi_y(t)$, where the effective noises are $\xi_x(t) = v_0 \cos \phi(t)$ and $\xi_y(t) = v_0 \sin \phi(t)$. Unlike the white noises in the PBP

that are independent of each other and uncorrelated in time, the active noises $\xi_x(t)$ and $\xi_y(t)$ are (a) correlated with each other and (b) correlated in time. For example the autocorrelation function of $\xi_x(t)$ is given by [35]

$$\langle \xi_x(t_1)\xi_x(t_2) \rangle \approx \frac{v_0^2}{2} \exp[-D_R|t_1 - t_2|], \quad (2)$$

for large t_1 and t_2 with $|t_1 - t_2|$ fixed and similarly for $\xi_y(t)$. It follows from Eq. (2) that for times $t \gg D_R^{-1}$, the autocorrelator converges to $\langle \xi_x(t_1)\xi_x(t_2) \rangle \rightarrow 2D_{\text{eff}}\delta(t_1 - t_2)$ with an effective diffusion constant $D_{\text{eff}} = v_0^2/(2D_R)$. Hence, for $t \gg D_R^{-1}$, the ABP effectively reduces to a PBP. Thus D_R^{-1} plays the role of an ‘activity’ parameter – as D_R increases from zero, the process crosses over from a strongly active regime ($D_R \rightarrow 0$) to a strongly passive one ($D_R \rightarrow \infty$).

One of the simplest and natural questions in the ABP dynamics is: how does the spatial distribution $P(x, y, t)$ evolve with time? In the case of a PBP, starting initially at the origin, this is simply a Gaussian at all times t :

$$P(x, y, t) = \frac{1}{4\pi Dt} e^{-(x^2+y^2)/4Dt}. \quad (3)$$

How does the presence of the internal degree of freedom $\phi(t)$ in Eq. (1) affect $P(x, y, t)$? In principle, $P(x, y, t)$ can be obtained as the marginal distribution:

$$P(x, y, t) = \int_{-\infty}^{\infty} d\phi \mathcal{P}(x, y, \phi, t), \quad (4)$$

where $\mathcal{P}(x, y, \phi, t)$ is the probability density in the (x, y, ϕ) space and satisfies the Fokker-Planck equation,

$$\frac{\partial}{\partial t} \mathcal{P}(x, y, \phi, t) = -v_0 \left[\cos \phi \frac{\partial \mathcal{P}}{\partial x} + \sin \phi \frac{\partial \mathcal{P}}{\partial y} \right] + D_R \frac{\partial^2 \mathcal{P}}{\partial \phi^2}. \quad (5)$$

However, this Fokker-Planck equation turns out to be very hard to solve explicitly. Thus, despite the simplicity of the ABP dynamics, extracting the explicit form of $P(x, y, t)$ in real space remains a challenging problem.

Recently, Kurzthaler *et al.* derived [36] an exact expression for the Fourier transform $\langle e^{-i\vec{k}\cdot\vec{r}(t)} \rangle$, where $\vec{r}(t) = (x(t), y(t))$, in terms of the eigenvalues and eigenfunctions of the Mathieu equation (see Sec. II below for details). In their derivation, $\langle \dots \rangle$ includes an averaging over all possible initial orientations $\phi(0)$, chosen uniformly at random. Consequently, this Fourier transform depends only on the magnitude k of the wave vector \vec{k} . However, this expression, although exact at all times, is still rather formal and inverting this Fourier transform to extract and plot $P(x, y, t)$ in the real x - y plane is far from obvious.

In a recent paper [35], using a backward Feynman-Kac approach we were able to derive, for any fixed initial orientation $\phi(0)$, exact and explicit expressions for the marginal distributions $P(x, t)$, $P(y, t)$ and $P(r^2, t)$ at short-times $t \ll D_R^{-1}$. A fixed initial condition makes the

x and y motion for the ABP *anisotropic*, especially at early times $t \ll D_R^{-1}$. This is manifest in the marginal distributions $P(x, t)$ and $P(y, t)$ which are completely different from each other at early times [35]. For example, for the initial condition $\phi(0) = 0$, it was shown that, for $t \ll D_R^{-1}$, the marginal distribution $P(y, t)$ has a simple Gaussian form

$$P(y, t) = \frac{1}{\sqrt{2\pi\sigma_y^2}} e^{-y^2/(2\sigma_y^2)}, \text{ with } \sigma_y^2 = \frac{2v_0^2 D_R t^3}{3}. \quad (6)$$

In contrast, the marginal $P(x, t)$, for $t \ll D_R^{-1}$, has a completely different expression given by the scaling form

$$P(x, t) = \frac{1}{v_0 D_R t^2} f_x \left(\frac{v_0 t - x}{v_0 D_R t^2} \right), \quad (7)$$

where the scaling function $f_x(z)$ is non-trivial and was computed explicitly in [35]. Note that the standard deviation of x grows as t^2 , while that of y grows as $t^{3/2}$, leading to anomalous super diffusion for both coordinates at early times. Both the anisotropy and the anomalous diffusion at early times were proposed as strong signatures of ‘activity’ of the ABP dynamics [35].

The picture, however, is quite different, at long times $t \gg D_R^{-1}$. At long times one expects that the system forgets the initial condition – hence the anisotropy disappears, and moreover by the central limit theorem normal diffusion is restored with an effective diffusion constant $D_{\text{eff}} = v_0^2/(2D_R)$ [3, 5, 35]. This indicates that for $t \gg D_R^{-1}$, the *typical* behaviour of $P(x, y, t)$ is described by the Gaussian form as in Eq. (3) with an effective diffusion constant $D = D_{\text{eff}} = v_0^2/(2D_R)$. The question remains whether it is possible to see any signature of the activity in this long time regime, apart from just a trivial renormalization of the diffusion constant.

The purpose of this paper is two-fold. In the first part, we show that the same backward Feynman-Kac approach that we had used earlier in Ref. [35] to derive the early time dynamics ($t \ll D_R^{-1}$), can be extended to derive explicitly $P(x, y, t)$ at late times $t \gg D_R^{-1}$. We show that, while the distribution near its peak is Gaussian describing the probability of typical fluctuations as expected, it has non-trivial non-Gaussian tails describing atypical rare fluctuations when $r = \sqrt{x^2 + y^2} \sim v_0 t$. On this scale, we show that $P(x, y, t)$ admits a large deviation form,

$$P(x, y, t) \sim \exp \left[-t D_R \Phi \left(\frac{\sqrt{x^2 + y^2}}{v_0 t} \right) \right], \quad (8)$$

where the rate function $\Phi(z)$ is supported over $z \in [0, 1]$. In this paper, we compute $\Phi(z)$ analytically. Computing $\Phi(z)$ from numerical simulations is also challenging as it requires measuring extremely small probabilities of rare fluctuations. In this paper we estimate $\Phi(z)$ from numerical simulations with extreme precision by adapting the importance sampling method and find a perfect

agreement with our analytical result (see Fig. 3). Our main conclusion is that at late times, while there is no trace of activity in the central Gaussian peak, the tails of the distribution still carry signatures of activity that is encoded in the rate function $\Phi(z)$.

We note that the marginal distribution $P(x, t)$ was studied in Ref. [30] and a similar large deviation form as in Eq. (8) was found,

$$P(x, t) \sim \exp \left[-t D_R \Phi_x \left(\frac{x}{v_0 t} \right) \right], \quad (9)$$

where the rate function $\Phi_x(z)$ is supported over $z \in [-1, 1]$ and is symmetric around $z = 0$. While this rate function $\Phi_x(z)$ was found to be related to the lowest eigenvalue of the Mathieu equation via a Legendre transform, the asymptotic behaviors of $\Phi_x(z)$ were not extracted. Interestingly, the same rate function $\Phi_x(z)$ was also found in the current distribution of an interacting active particle system [37], within an effective mean-field description, that just renormalises the single particle velocity v_0 which now depends on the density ρ – still, the asymptotic properties of $\Phi_x(z)$ were not analysed. In this paper, we show that, for $z \in [0, 1]$, the rate function $\Phi(z)$ in Eq. (8) describing the two-dimensional probability distribution, indeed coincides with $\Phi_x(z)$ in Eq. (9) and we provide the asymptotic behavior of $\Phi(z)$ both as $z \rightarrow 0$ and $z \rightarrow 1$.

In the second part of the paper we consider another way to detect the signatures of activity at late times, by subjecting the ABP to an external harmonic potential of stiffness μ . Here the system approaches a stationary state at long times $P_{\text{stat}}(x, y) = P(x, y, t \rightarrow \infty)$. This stationary distribution changes its character as a function of the activity parameter D_R^{-1} . In the strongly active limit $D_R \rightarrow 0$, the stationary distribution is highly non-Gaussian and has a ring shape of radius v_0/μ . In contrast, in the weakly active regime $D_R \rightarrow \infty$, the stationary distribution has a Gaussian shape. We study, both numerically and analytically, this crossover in the shape of $P_{\text{stat}}(x, y)$ as a function of the activity parameter D_R^{-1} .

The rest of the paper is organized as follows. In Sec. II we discuss an elegant geometrical interpretation of the ABP dynamics in terms of a random algebraic curve in two dimensions and provide a detailed summary of our main results. In Sec. III we compute the rate function $\Phi(z)$, both analytically and numerically. Sec. IV is devoted to the study of the ABP in a harmonic trap. Finally we conclude in Sec. V. Some details of the calculations are relegated to the four Appendices.

II. THE MODEL AND THE SUMMARY OF THE RESULTS

The ABP model has already been defined in Eq. (1) in the Introduction. We assume that the particle starts at the origin $x = y = 0$, with a given initial orientation $\phi(0)$.

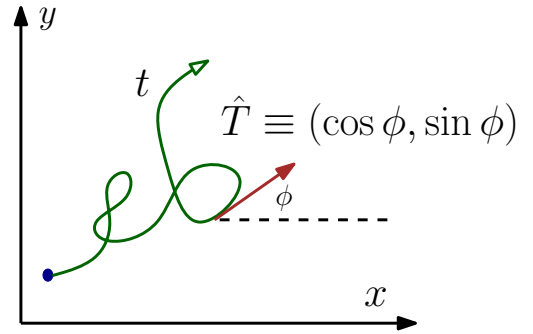


FIG. 2. Geometric interpretation of the ABP as a two dimensional algebraic curve with random curvature [47].

We are interested in calculating the distribution $P(x, y, t)$ at late times $t \gg D_R^{-1}$. Before summarizing our main results, it is useful to first make a historical remark that will also provide an elegant geometrical representation of the ABP.

It turns out that much before the ABP model appeared in the literature of active self-propelled particles, Eq. (1) was already introduced and studied in the mathematics literature by Mumford in a completely different context [47]. Mumford was interested in the properties of two dimensional random algebraic curves in the context of computer vision. Consider a continuous curve $\{x(t), y(t)\}$ in $2d$, where t denotes the arc length along the curve (see Fig. 2 for a schematic representation). Thus t increases monotonically as one moves along the curve. Let $\hat{T} \equiv (\cos(\phi(t)), \sin(\phi(t)))$ denote the unit tangent vector to the curve at arc distance t , where $\phi(t)$ represents the angle between \hat{T} and the x axis. Hence the coordinates $(x(t), y(t))$ of the curve are expressed in terms of the angle $\phi(t)$ via

$$x(t) = \int_0^t ds \cos \phi(s), \quad y(t) = \int_0^t ds \sin \phi(s). \quad (10)$$

Let $\kappa(t)$ denote the local curvature at arc distance t . Consequently the local radius of curvature $R(t) = 1/\kappa(t)$. Consider an infinitesimal evolution of the curve from t to $t + dt$. Clearly $R(t)d\phi = dt$ and this gives $\kappa(t) = \frac{d\phi}{dt}$. Mumford proposed a ‘random curvature model’ for the algebraic curve where $\kappa(t)$ is a delta correlated white noise with zero mean. As a result, $\phi(t)$ in this random curvature model is just a Brownian motion with arc length t playing the role of time. Hence the random curve described by Eq. (10) is exactly equivalent to an ABP in Eq. (1) with $v_0 = 1$. Mumford was precisely interested in calculating $P(x, y, t)$ and wrote down the Fokker-Planck Eq. (5). However, he was not able to solve it and remarked “I have looked for an explicit formula for P but in vain” [47].

As mentioned in the Introduction, a recent progress was made in Ref. [36], where the authors derived an exact

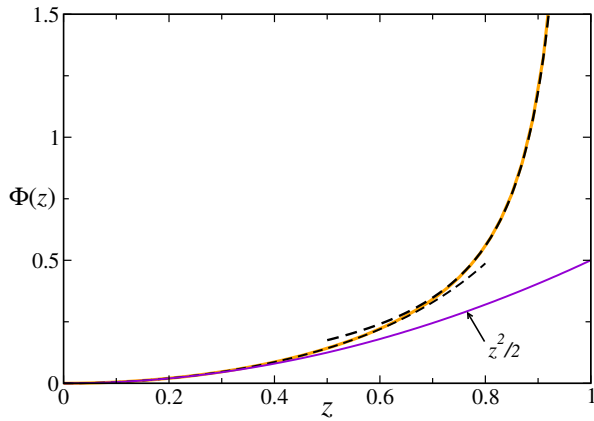


FIG. 3. The rate function $\Phi(z)$ supported over $z \in [0, 1]$. The solid (orange) line corresponds to the exact expression given in Eq. (12) evaluated using the Mathematica. The dashed lines correspond to the explicit asymptotic expansions in Eq. (14). The solid (violet) line with the quadratic behaviour $z^2/2$ corresponds to passive Brownian particle.

expression for the Fourier transform $f(k, t) = \langle e^{-i\vec{k} \cdot \vec{r}(t)} \rangle$, where the average is also performed over all initial orientations of the angle $\phi(0)$ chosen uniformly in the range $[-\pi, \pi]$. Consequently the Fourier transform depends only on the magnitude k of the wave vector \vec{k} and the distribution in real space is isotropic at all times t . Ref. [36] derived $f(k, t)$ in the presence of an additional translational noise in Eq. (1). Upon setting this additional noise to zero, their result reads,

$$f(k, t) = \sum_{n=0}^{\infty} e^{-\lambda_{2n} t} \left[\int_0^{2\pi} \frac{d\varphi}{2\pi} \text{ce}_{2n} \left(\frac{\varphi}{2}, \frac{2ikv_0}{D_R} \right) \right]^2, \quad (11)$$

where $\text{ce}_{2n}(v, q)$ are solutions of the Mathieu equation, π -periodic and even in v , with eigenvalue $a_{2n}(q)$ (see Section III for more details), and $\lambda_{2n} = a_{2n}(\frac{2ikv_0}{D_R}) \frac{D_R}{4}$. Although exact for all t in the \vec{k} space, extracting the behavior of $P(x, y, t)$ in real space is non-trivial and has not been done so far.

In this paper, using an alternative backward Feynman-

Kac formalism, we obtain an exact expression valid at all times for the moment generating function of $P(x, y, t)$ —similar to $f(k, t)$ above but with imaginary k . However, our solution is valid for arbitrary initial condition $\phi(0)$ [see Eq. (25)]. Next, for large times ($t \gg D_R^{-1}$), we extract explicitly from this moment generating function the behaviour of $P(x, y, t)$ in real space. In particular we show that at late times the probability density admits a large deviation form as in Eq. (8) in the Introduction, that describes the non-Gaussian tails of the distribution in the real space. We show that the rate function $\Phi(z)$ can be expressed as the Legendre transform of the lowest eigenvalue a_0 associated with the π -periodic even solution of the Mathieu equation:

$$\min_{0 \leq z \leq 1} \left[\frac{p}{D_R} z + \Phi(z) \right] = \frac{1}{4} a_0 \left(\frac{2p}{D_R} \right). \quad (12)$$

The rate function $\Phi(z)$ is supported over the interval $z \in [0, 1]$. Note that $\Phi(z)$ depends only on the scaled radius $z = \sqrt{x^2 + y^2}/(v_0 t)$. This indicates that $-\ln P(x, y, t)$ becomes completely isotropic at late times and does not depend on the initial orientation $\phi(0)$. Hence even the marginals, such as $P(x, t)$, has the asymptotic form

$$P(x, t) \sim \exp \left[-t D_R \Phi_x \left(\frac{x}{v_0 t} \right) \right], \quad (13)$$

where $\Phi_x(z)$ is supported over the interval $z = x/(v_0 t) \in [-1, 1]$ and is symmetric around $z = 0$. For positive z , using the isotropy, we have $\Phi_x(z) = \Phi(z)$, where $\Phi(z)$ is given in Eq. (12). Thus the rate function $\Phi(z)$ can also be extracted from the late time behaviour of just the marginal $P(x, t)$, which turns out to be somewhat easier to analyse. For the simplicity of notation, henceforth we will drop the subscript x from $\Phi_x(z)$. As mentioned in the introduction, this result in Eq. (13) already appeared in Refs. [30, 37], though the detailed analytical form of $\Phi(z)$ was not carried out. In this paper, we show that the asymptotic behaviours of $\Phi(z)$ as $z \rightarrow 0$ and $z \rightarrow 1$ can be extracted from Eq. (12) using the known asymptotic properties of $a_0(q)$ and we obtain

$$\Phi(z) = \begin{cases} \frac{1}{2} z^2 + \frac{7}{32} z^4 + \frac{209}{1152} z^6 + \frac{53231}{294912} z^8 + \dots & \text{as } z \rightarrow 0 \\ \frac{1}{8(1-z)} - \frac{1}{16} - \frac{(1-z)}{64} - \frac{3}{256} (1-z)^2 - \frac{51}{4096} (1-z)^3 + \dots & \text{as } z \rightarrow 1 \end{cases} \quad (14)$$

A plot of $\Phi(z)$ is given in Fig. 3. In Sec. III we further compute numerically the marginal $P(x, t)$ (see Fig. 4) using an importance sampling method. From this marginal we extract the rate function $\Phi(z)$ numerically, as shown in Fig. 5, finding excellent agreement with our analytical prediction.

In the second part of the paper we study the position distribution $P_\mu(x, y, t)$ of the ABP trapped in a harmonic potential of stiffness μ . In this case we derive an exact recursion relation in Eq. (61), valid at all times t , for the moments $M_{kl}(t) = \langle z^k(t) \bar{z}^l(t) \rangle$ where $z(t) = x(t) + iy(t)$. We show that this recursion relation can be solved

explicitly for all t in the two opposite limits: (a) the strongly active limit, i.e. when $D_R \rightarrow 0$ and (b) the strongly passive limit, i.e. when $D_R \rightarrow \infty$. From these exact moments we derive, in these two limiting cases, the exact radial distribution *at all times* t

$$P_{\text{rad}}(r, t) = \int_0^{2\pi} P_\mu(r, \theta, t) d\theta. \quad (15)$$

where $P_\mu(r, \theta, t)$ is the position distribution in the polar coordinates. We show that in the strongly active limit ($D_R \rightarrow 0$), the stationary position distribution at long times approaches a ring shape in the x - y plane of radius v_0/μ . In contrast, in the strongly passive regime ($D_R \rightarrow \infty$), the stationary distribution is a Gaussian

$$P_{\text{stat}}(x, y) = \frac{\mu D_R}{\pi v_0^2} \exp\left[-\frac{\mu D_R (x^2 + y^2)}{v_0^2}\right]. \quad (16)$$

For intermediate values of D_R , we study the stationary distribution $P_{\text{stat}}(x, y)$ numerically and find that as D_R increases, $P_{\text{stat}}(x, y)$ crosses over from the ring shape to the Gaussian shape as displayed in Fig. 7.

III. POSITION DISTRIBUTION AT LATE TIMES: LARGE DEVIATION

In this Section we study the behaviour of the position probability distribution $P(x, y, t)$ of an ABP at late times $t \gg D_R^{-1}$. We consider Eq. (1) and assume that the particle starts at the origin $x(0) = y(0) = 0$. For a fixed initial orientation $\phi(0) = u$, the radial symmetry is broken and consequently the coordinates $x(t) = v_0 \int_0^t d\tau \cos \phi(\tau)$ and $y(t) = v_0 \int_0^t d\tau \sin \phi(\tau)$ will have different statistical behaviours, especially at early times. At late times, for typical fluctuations, this anisotropy is expected to disappear and one would recover the isotropic Gaussian distribution as in Eq. (3) with the effective diffusion constant $D_{\text{eff}} = v_0^2/(2D_R)$. Here we are interested in the atypical large fluctuations in the tails of the distribution $P(x, y, t)$, where $\sqrt{x^2 + y^2} \sim v_0 t$. We show that these atypical fluctuations also become isotropic, at least to leading order at large t , and $P(x, y, t)$ is described by the large deviation form as in Eq. (8) where the rate function depends only on $z = \sqrt{x^2 + y^2}/(v_0 t)$.

To compute these atypical fluctuations of $P(x, y, t)$ it turns out to be convenient to first study the marginal distribution $P_u(x, t) = \int dy P(x, y, t)$, where $x(t) = v_0 \int_0^t d\tau \cos \phi(\tau)$ and $\phi(0) = u \in (-\pi, \pi)$. For convenience, we further rescale the x -coordinate and define $w(t) = x(t)/v_0 = \int_0^t d\tau \cos \phi(\tau)$. Therefore, $P_u(x, t) = (1/v_0) P_u(w, t)$. Thus $w(t)$ is just a functional of a one dimensional Brownian motion $\phi(t)$ that starts at $\phi(0) = u$. The statistical properties of such Brownian functionals can be very conveniently derived by using a backward Feynman-Kac approach where one treats the initial condition $\phi(0) = u$ as a variable – for several examples

and applications, see Ref. [48]. A key quantity for this method turns out to be the moment generating function

$$Q_p(u, t) = \left\langle e^{-p \int_0^t d\tau \cos \phi(\tau)} \right\rangle = \int_{-t}^t dw e^{-pw} P_u(w, t), \quad (17)$$

where we note that the range of w is $\in [-t, t]$. For the functional $w(t) = \int_0^t d\tau \cos \phi(\tau)$, the backward Feynman-Kac equation for the moment generating function $Q_p(u, t)$ then reads [48],

$$\frac{\partial Q_p}{\partial t} = D_R \frac{\partial^2 Q_p}{\partial u^2} - p \cos u Q_p, \quad (18)$$

with the initial condition $Q_p(u, t = 0) = 1$. Equation (18) is just the Schrödinger equation in imaginary time for a particle in a periodic potential $\cos u$. We look for a solution of the form $e^{-\lambda t} \psi(u)$. Then Eq. (18) becomes,

$$D_R \frac{d^2 \psi}{du^2} + (\lambda - p \cos u) \psi(u) = 0 \quad (19)$$

where the physical solution should be periodic with a period 2π (recall that $u = \phi(0) \in (-\pi, \pi)$),

$$\psi(u) = \psi(u + 2\pi). \quad (20)$$

It turns out that the above equation can be recast as the standard Mathieu equation [49] with a rescaling $u = 2v$,

$$\psi''(v) + (a - 2q \cos 2v) \psi(v) = 0, \quad (21)$$

where $a = 4\lambda/D_R$ and $q = 2p/D_R$. Note that the periodicity condition in Eq. (20) translates in the variable v to

$$\psi(v) = \psi(v + \pi). \quad (22)$$

For any fixed q , the Mathieu equation (21) admits four families of periodic solutions for a discrete set of values of the parameter a called characteristic values, or eigenvalues [49]:

- the elliptic cosine $\text{ce}_{2n}(v, q)$, π -periodic and even function in v with eigenvalues $a = a_{2n}(q)$;
- the elliptic cosine $\text{ce}_{2n+1}(v, q)$, 2π -periodic and even function in v with eigenvalues $a = a_{2n+1}(q)$;
- the elliptic sine $\text{se}_{2n}(v, q)$, π -periodic and odd function in v with eigenvalues $a = b_{2n}(q)$;
- the elliptic sine $\text{se}_{2n+1}(v, q)$, 2π -periodic and odd function in v with eigenvalues $a = b_{2n+1}(q)$.

The condition in Eq. (22) allows only the π -periodic solutions, $\text{ce}_{2n}(v, q)$ and $\text{se}_{2n}(v, q)$. The general solution of Eq. (19), satisfying Eq. (20), can then be written as,

$$Q_p(u, t) = \sum_{n=0}^{\infty} A_{2n} \text{ce}_{2n}\left(\frac{u}{2}, \frac{2p}{D_R}\right) e^{-\frac{t D_R}{4} a_{2n}\left(\frac{2p}{D_R}\right)} + \sum_{n=0}^{\infty} B_{2n} \text{se}_{2n}\left(\frac{u}{2}, \frac{2p}{D_R}\right) e^{-\frac{t D_R}{4} b_{2n}\left(\frac{2p}{D_R}\right)}$$

The coefficients A_{2n} and B_{2n} can be determined from the initial condition. Setting $t = 0$ and using the orthogonality of the elliptic cosine and sine functions one gets:

$$A_{2n} \propto \int_{-\pi}^{\pi} Q_p(u, 0) \text{ce}_{2n} \left(\frac{u}{2}, \frac{2p}{D_R} \right) du \quad (23)$$

$$B_{2n} \propto \int_{-\pi}^{\pi} Q_p(u, 0) \text{se}_{2n} \left(\frac{u}{2}, \frac{2p}{D_R} \right) du, \quad (24)$$

where the proportionality factors are just the normalization of ce_{2n} and se_{2n} respectively. Using the initial condition $Q_p(u, t = 0) = 1$ and the parity of the functions ce_{2n} and se_{2n} , we immediately see that $B_{2n} = 0$ while $A_{2n} \neq 0$. Therefore we finally get

$$Q_p(u, t) = \sum_{n=0}^{\infty} A_{2n} \text{ce}_{2n} \left(\frac{u}{2}, \frac{2p}{D_R} \right) e^{-\frac{t D_R}{4} a_{2n} \left(\frac{2p}{D_R} \right)} \quad (25)$$

Clearly the dependence on the initial condition u appears only in the eigenfunctions ce_{2n} , *but not in the eigenvalues* a_{2n} .

At late times $t \gg D_R^{-1}$, one can make progress since the solution in Eq. (25) is dominated by the smallest eigenvalue $a_0(q)$ and we get

$$Q_p(u, t) \sim \exp \left[-\frac{t D_R}{4} a_0 \left(\frac{2p}{D_R} \right) \right]. \quad (26)$$

It is important to remark that in this limit the argument of the exponential is independent of the initial condition u (only the prefactor, which is sub-dominant in t , depends on u). The behaviour of $a_0(q)$ is known both for $q \rightarrow 0$ and $q \rightarrow \infty$ limits:

$$a_0(q) = \begin{cases} \sum_{n=1}^{\infty} \alpha_{2n} q^{2n} & \text{for } q \rightarrow 0 \\ \sum_{n=0}^{\infty} \beta_n q^{1-\frac{n}{2}} & \text{for } q \rightarrow \infty. \end{cases} \quad (27)$$

Explicit values of α_{2n} and β_n are known [49] and are quoted in the Appendix A. This allows us to extract both the cumulants and the large deviation function of the x -coordinate of the particle position, as we now show.

Let us recall that $Q_p(u, t) = \langle \exp(-px(t)/v_0) \rangle$ is the moment generating function of $w = x/v_0$. More precisely, expanding the $\ln Q_p(u, t)$ in powers of p gives

$$\ln Q_p(u, t) = \sum_{n=1}^{\infty} \frac{(-p)^n}{n!} \frac{\langle x^n \rangle_c}{v_0^n}, \quad (28)$$

where $\langle x^n \rangle_c$ denotes the n -th cumulant of x . To leading order in large t , taking the logarithm of $Q_p(u, t)$ in Eq. (26) gives

$$\log Q_p(u, t) \approx -\frac{t D_R}{4} a_0 \left(\frac{2p}{D_R} \right). \quad (29)$$

Next we use the small p expansion of $a_0 \left(\frac{2p}{D_R} \right)$ in Eq. (27) and match powers of p to extract the cumulants in Eq. (28). To leading order in large t , this gives for the even cumulants

$$\langle x^{2n} \rangle_c \approx -\alpha_{2n} \frac{(2n)!}{4} \left(\frac{2v_0}{D_R} \right)^{2n} D_R t, \quad (30)$$

while the odd cumulants vanish to this leading order of t . Note that at this leading order for large t , the cumulants are already independent of the initial condition u . Using the known explicit values of α_{2n} [49], we get the first few cumulants explicitly to leading order for large t :

$$\begin{aligned} \langle x^2 \rangle_c &\approx \left(\frac{v_0}{D_R} \right)^2 D_R t \\ \langle x^4 \rangle_c &\approx -\frac{21}{4} \left(\frac{v_0}{D_R} \right)^4 D_R t \\ \langle x^6 \rangle_c &\approx 145 \left(\frac{v_0}{D_R} \right)^6 D_R t \\ \langle x^8 \rangle_c &\approx -\frac{2404045}{256} \left(\frac{v_0}{D_R} \right)^8 D_R t, \end{aligned} \quad (31)$$

in agreement with the results obtained in Refs. [30, 37] using the tilt-operator method due to Lebowitz and Spohn [50], which, for Brownian motion, is equivalent to the forward Feynman-Kac formalism. Note that the sign of the even cumulants oscillate with increasing n . Since the odd cumulants vanish in this long-time limit, they leave no trace of the initial anisotropy for large t . However, the presence of non-zero higher order even cumulants already indicates that the tails of the distribution are non-Gaussian.

To extract the large deviation behaviour of the marginal $P(x, t)$ from its moment generating function in Eq. (26) we proceed as follows. For fluctuations on a scale $x \sim v_0 t$, we anticipate the large deviation form (to be verified a posteriori)

$$P(x, t) \sim \exp \left[-t D_R \Phi \left(\frac{x}{v_0 t} \right) \right] \quad (32)$$

where $\Phi(z)$ is the rate function, supported over the interval $z \in (-1, 1)$. In terms of the rescaled variable $z = x/(v_0 t) = w/t$, the moment generating function is $Q_p(u, t) = \langle \exp(-px/v_0) \rangle = \langle \exp(-ptz) \rangle$. Substituting the anticipated form Eq. (32) for $P(x, t)$ (or equivalently for $P(z, t)$) in Eq. (17) gives

$$Q_p(u, t) \sim \int_{-1}^1 dz \exp \left\{ -t D_R \left[\frac{p}{D_R} z + \Phi(z) \right] \right\}. \quad (33)$$

For large t , evaluating the integral by the saddle point method we get,

$$Q_p(u, t) \sim \exp \left\{ -t D_R \min_{-1 \leq z \leq 1} \left[\frac{p}{D_R} z + \Phi(z) \right] \right\}. \quad (34)$$

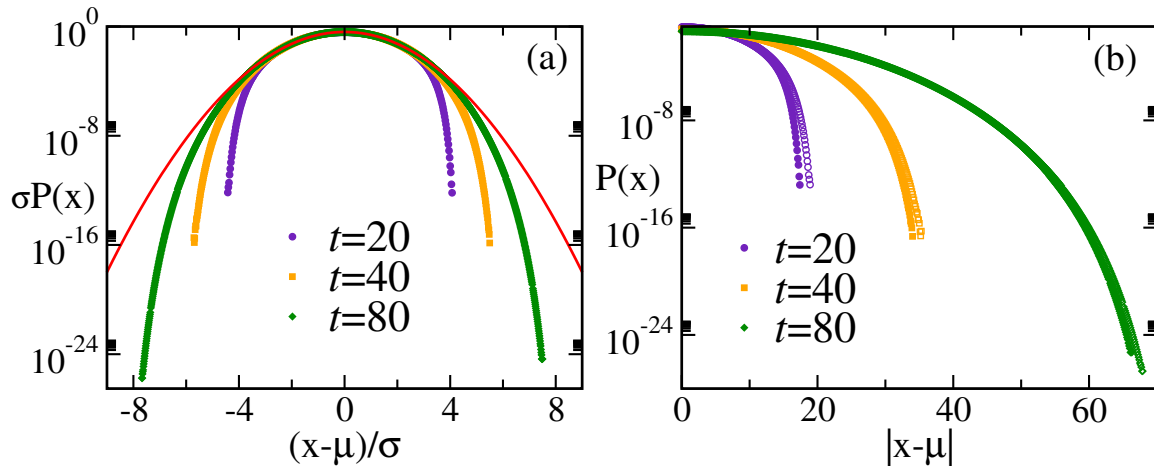


FIG. 4. Marginal distribution $P(x, t)$ for different (large) values of $t = 20, 40, 80$ obtained from numerical simulations using importance sampling. (a) The dimensionless probability density $\sigma_x P(x, t)$ plotted as a function of the centered and rescaled position $(x(t) - \langle x(t) \rangle) / \sigma_x$, where, $\sigma_x = \sqrt{\langle x^2 \rangle - \langle x \rangle^2}$ is the standard deviation. For comparison, we have shown the pure Gaussian distribution by the solid (red) line. (b) $\sigma_x P(x, t)$ plotted as a function of $|x(t) - \langle x(t) \rangle|$ to emphasize the asymmetry between $P(x, t)$ and $P(-x, t)$. The solid and open symbols correspond to the $x(t) > \langle x(t) \rangle$ and $x(t) < \langle x(t) \rangle$ respectively. The two branches become identical as t increases, indicating the symmetric distribution in the $t \rightarrow \infty$ limit.

Comparing Eq. (26) and Eq. (34), we get,

$$\min_{-1 \leq z \leq 1} \left[\frac{p}{D_R} z + \Phi(z) \right] = \frac{1}{4} a_0 \left(\frac{2p}{D_R} \right). \quad (35)$$

Inverting this Legendre transform, the rate function $\Phi(z)$ can be finally expressed as

$$\Phi(z) = \max_p \left[\frac{1}{4} a_0 \left(\frac{2p}{D_R} \right) - \frac{zp}{D_R} \right]. \quad (36)$$

The eigenvalue $a_0(q = 2p/D_R)$ is a symmetric function of q . Hence it follows immediately from Eq. (36) that $\Phi(z) = \Phi(-z)$. While Eq. (36) has appeared before in the literature [30, 37], its behavior for $z \rightarrow 0$ as well as $z \rightarrow \pm 1$ was not extracted. Here we use the asymptotic expansions of $a_0(q)$, both for small and large q in Eq. (27), to determine the limiting behaviors of $\Phi(z)$ as $z \rightarrow 0$ and $z \rightarrow 1$ respectively. The details are provided in the Appendix B and the explicit limiting behaviors of $\Phi(z)$ are given in Eq. (14) of Sec. II. In Fig. 3, we provide a plot of $\Phi(z)$ for $z \in [0, 1]$ (note that $\Phi(z) = \Phi(-z)$).

So far we have studied the marginal $P(x, t)$ and observed that to leading order in large t , $-\ln P(x, t)$ is independent of the initial condition u . This means that one would observe the same rate function $\Phi(z)$ for the marginal distribution along any axis, and not just for $P(x, t)$. As a consequence $-\ln P(x, y, t)$ would also be described by the same rate function $\Phi(z)$ with $z = \sqrt{x^2 + y^2} / (v_0 t) \in (0, 1)$. This gives the large deviation form for $P(x, y, t)$ as announced in Eq. (8) in the Introduction. The rate function $\Phi(z)$ associated with $P(x, y, t)$ is thus the same as in Eq. (36), but with its argument $z \in (0, 1)$. Note that the large deviation form in Eq. (8) not only contains the probability of extremely large fluctuations of order $r = \sqrt{x^2 + y^2} \sim v_0 t$,

but also the typical fluctuations where $r \sim \sqrt{t}$. To see this, we note that for $r \sim \sqrt{t}$, the scaled variable $z = r / (v_0 t) \sim O(1/\sqrt{t})$ and hence is very small for large t . Using the quadratic form of $\Phi(z) \sim z^2/2$ near $z = 0$ in the small z expansion in Eq. (14) and substituting this in Eq. (8), one recovers the typical Gaussian fluctuations

$$P(x, y, t) \sim e^{-(x^2 + y^2) / 4D_{\text{eff}} t}. \quad (37)$$

with $D_{\text{eff}} = v_0^2 / (2D_R)$.

We close this discussion with a final remark. We note that the result for $\Phi(z)$ in Eq. (36) could also have been derived directly from the result of Kurzthaler et. al. in Eq. (11). However, we presented here an alternative derivation based on the backward Feynman-Kac approach for two reasons. First, our result in Eq. (25) is valid for arbitrary initial condition $\phi(0)$ and demonstrates, in particular, how the dependence on the initial condition disappears at late times, leading to an isotropic tail of the position distribution $P(x, y, t)$ in the x - y plane in Eq. (8), with a rate function that only depends on the rescaled radial distance $z = \sqrt{x^2 + y^2} / (v_0 t)$. Secondly, we wanted to develop a single unifying method that is able to provide explicitly $P(x, y, t)$ both at early times $t \ll D_R^{-1}$ [35] as well as at late times $t \gg D_R^{-1}$ – our approach based on the backward Feynman-Kac formalism does exactly that.

A. Numerical Measurement of the Large Deviation Function

The dynamics of the ABP is also simulated numerically to measure the position probability distribution and the large deviation functions. For measuring the moments

and distributions in the typical regime one can use the standard Euler's method where the Langevin equations are discretized as,

$$\begin{aligned} x(t+dt) &= x(t) + v_0 \cos \phi(t) dt \\ y(t+dt) &= y(t) + v_0 \sin \phi(t) dt \\ \phi(t+dt) &= \phi(t) + \sqrt{2D_R} dt \eta_\phi(t) \end{aligned} \quad (38)$$

where $\eta_\phi(t)$, for each t , is an independent random number drawn from the zero mean unit variance Gaussian distribution. We start from the fixed initial condition $\phi(0) = 0$, set $dt = 10^{-3}$ and 10^{-4} , $v_0 = D_R = 1$ and measure only the marginal distribution $P(x, t)$ for different values of t (for this we do not need to monitor the y coordinate). Since $\phi(0) = 0$, the average value of x is nonzero and is given by [35]

$$\langle x(t) \rangle = \langle \cos \phi(t) \rangle = \frac{v_0}{D_R} (1 - e^{-D_R t}). \quad (39)$$

Note that when we monitor $P(x, t)$ we actually plot it as a function of $x(t) - \langle x(t) \rangle$.

Using this standard Euler method of integrating the Langevin equation, we can easily sample 10^8 realizations. This limits the smallest probabilities which can be resolved to be $> 10^{-8}$. To estimate $P(x, t)$ when its value is much smaller, e.g., when $P \sim 10^{-25}$, we use the *Importance Sampling* method. This approach has been successfully used to extract the tails of distributions with extremely small probabilities in a wide variety of problems [51–61]. The basic idea behind the importance sampling method is to sample trajectories (or configurations in general) ending at $x(t)$ with an additional exponential tilt $e^{-\theta x(t)}$, where θ is an adjustable parameter. Positive values of θ will bias the trajectories with very negative $x(t) \simeq -t$. Contrarily, negative θ samples trajectories ending near the other limit, *i.e.*, $x(t) \simeq t$.

Let $\mathcal{P}(\omega)$ denote the probability of the trajectory $\omega = \{x_s; 0 \leq s \leq t\}$ of the ABP during the time interval $[0, t]$. The expectation value of any observable $O(\omega)$ is given by

$$\langle O(\omega) \rangle_{\mathcal{P}} = \int \mathcal{D}\omega \mathcal{P}(\omega) O(\omega). \quad (40)$$

The presence of the tilt introduces a bias in the trajectory probabilities,

$$\mathcal{Q}(\omega) = \mathcal{P}(\omega) \frac{e^{-\theta x(t)}}{Z_\theta} \quad (41)$$

where Z_θ is the normalization constant which depends only on θ and t . The expectation value $\langle O(\omega) \rangle_{\mathcal{P}}$ can be computed from this tilted ensemble by reweighing the observable,

$$\langle O(\omega) \rangle_{\mathcal{P}} = \int \mathcal{D}\omega \tilde{O}(\omega) \mathcal{Q}(\omega) \quad (42)$$

where

$$\tilde{O}(\omega) = \frac{O(\omega) \mathcal{P}(\omega)}{\mathcal{Q}(\omega)} = e^{\theta x(t)} Z_\theta O(\omega). \quad (43)$$

In practice, a trajectory is completely specified by a sequence of $N = t/dt$ Gaussian random numbers η_i . In order to generate trajectories from the biased ensemble we rely on a Metropolis approach. Starting from an allowed trajectory ω ending at $x(t)$ we generate a trial tilted trajectory $\tilde{\omega}$ by modifying r fraction of the random numbers. The trial trajectory is accepted with a probability $P_{\text{Met}} = \min(1, e^{-\theta(\tilde{x}(t) - x(t))})$ where $\tilde{x}(t)$ denotes the ending point of the trial trajectory. The value of the parameter r is adjusted in order to have $P_{\text{Met}} \approx 0.5$ in average.

To measure the distribution $P(x, t)$ for a wide range of values of x , we change the value of the parameter θ . In the data presented in Figs. 4 and 5 we have used $\theta = \pm 0.75, \pm 1.5, \pm 2.0$ and ± 2.5 . The histogram obtained for each value of θ is shifted by an unknown amount Z_θ . To fix it, we use the histogram obtained from the standard Euler simulation, which is correctly normalized and accurate near the origin $x = 0$, and corresponds to $\theta = 0$. For the smallest negative (positive) value of θ , we match the histogram obtained from the biased sampling with the right (left) part of the $\theta = 0$ curve. We continue the same matching procedure for the subsequent values of θ to get the full curve $P(x, t)$.

The marginal distribution $P(x, t)$ thus obtained for different values of t are plotted in Fig. 4(a). As is visible from this plot, the importance sampling has allowed us to resolve $P(x, t)$ near the boundaries $x = \pm 1$ to an accuracy smaller than 10^{-25} for $t = 20$. Fig. 4(b) shows $P(x, t)$ plotted as a function of $|x(t) - \langle x(t) \rangle|$ which illustrates that the distribution becomes symmetric around the mean as t increases.

The large deviation function $\Phi(x/v_0 t)$ is extracted from the $P(x, t)$ obtained from numerical simulations following,

$$\Phi(x/v_0 t) = -\frac{1}{D_R t} [\log P(x, t) - \log P(0, t)] \quad (44)$$

This ensures that $\Phi(0) = 0$. This is plotted in Fig 5 for different (large) values of t . The symbols correspond to the data obtained from numerical simulations and lines correspond to the asymptotic expansions of the rate function $\Phi(z)$ in Eq. (14). The agreement between the numerical data and the analytical curves, both near $z = 0$ and $z = \pm 1$, improves as t increases, validating our prediction.

The non-trivial behaviour of the large deviation function is one clear sign of 'activeness' of ABP at late times. As already mentioned, another, more direct, way to explore the 'active' regime is to put the ABP in an external potential. In the next section we investigate the behaviour of an ABP in a harmonic potential.

IV. ABP IN A HARMONIC TRAP

In this section we consider the behaviour of an ABP in the presence of a confining harmonic potential $U(x, y) =$

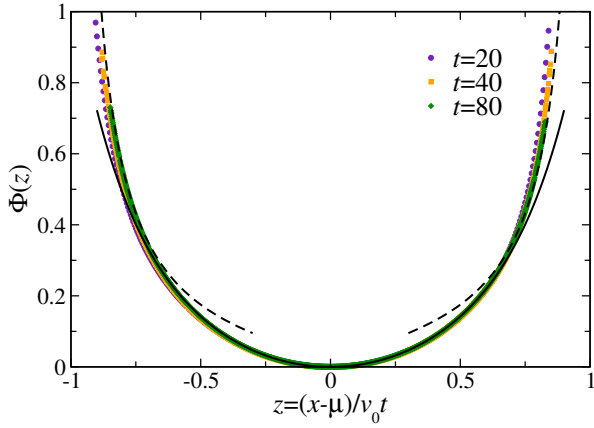


FIG. 5. The large deviation function $\Phi(z)$ vs $z = (x(t) - \langle x(t) \rangle)/v_0 t$ for three different values of t , as obtained from numerical simulations. The solid black line corresponds to the asymptotic behaviour near $z \rightarrow 0$ in Eq. (14). The dashed black lines correspond to asymptotic behaviour near $z \rightarrow \pm 1$ in Eq. (14).

$\mu(x^2 + y^2)/2$. In this case, the Langevin equations governing the dynamics of the particle become,

$$\begin{aligned} \dot{x} &= -\mu x + v_0 \cos \phi(t) \\ \dot{y} &= -\mu y + v_0 \sin \phi(t) \\ \dot{\phi} &= \sqrt{2D_R} \eta_\phi(t). \end{aligned} \quad (45)$$

The ABP in a harmonic trap has been extensively studied both theoretically and experimentally [23, 27, 31, 41, 42, 46]. In a recent experiment, Janus swimmers were confined in a two-dimensional harmonic-like trap with the use of an acoustic tweezer and the stationary density was measured by varying the trap strength [31]. Strong signatures of activity were observed even in the dilute limit, with a crossover from a Gaussian-like stationary state, to a strongly active stationary state, where the particles cluster at the outskirts of the trap. The dilute limit corresponds to a collection of non-interacting Active Brownian Particles (ABP) in a harmonic potential as in Eq. (45). Numerical studies of this model have also observed a similar crossover in the stationary state [23, 27].

Dynamical behaviour of an ABP differs crucially from that of a PBP, also in the presence of a harmonic potential. For a ‘passive’ or ordinary Brownian particle, the presence of a harmonic trap of strength μ sets a relaxational time scale μ^{-1} . At times $t \ll \mu^{-1}$, the particle diffuses isotropically and for $t \gg \mu^{-1}$, a Gaussian (Boltzmann) stationary distribution is reached. As explained before, for an ABP, the coupling to the rotational diffusion introduces an additional time scale D_R^{-1} , where D_R is the rotational diffusion constant.

While the activity induced crossover in the stationary position distribution of an ABP has been studied both experimentally and numerically, the interplay of the two

time scales μ^{-1} and D_R^{-1} leads to fascinating dynamical features as we demonstrate below. The physical picture emerging from our study is summarized in Fig. 6 for $D_R^{-1} < \mu^{-1}$ (upper panel) and for $D_R^{-1} > \mu^{-1}$ (lower panel). In both cases, at short-times $t \ll \min(D_R^{-1}, \mu^{-1})$, the presence of the activity gives rise to strong anisotropy with the particle retaining its initial orientation (chosen to be along x -direction here). In this regime, the effect of the trap can be neglected and the dynamics reduces to that of a free ABP. At later times, if $D_R^{-1} < \mu^{-1}$, the anisotropy starts to disappear and the ABP undergoes ordinary diffusion (upper middle panel). Eventually, for $t \gg \mu^{-1}$ the probability distribution saturates to a Boltzmann-like form with a single Gaussian peak at the center of the trap. On the other hand, for strongly active system, *i.e.*, when $D_R^{-1} > \mu^{-1}$ the anisotropy persists and the particle starts to accumulate away from the center of the trap. For $t \gg D_R^{-1}$ the isotropy is slowly recovered (lower right panel). The stationary distributions we obtain in the two limiting cases are in agreement with the experimental and numerical observations [27, 31].

The position distribution $P_\mu(x, y, t)$ can be obtained by integrating out the orientational degree of freedom

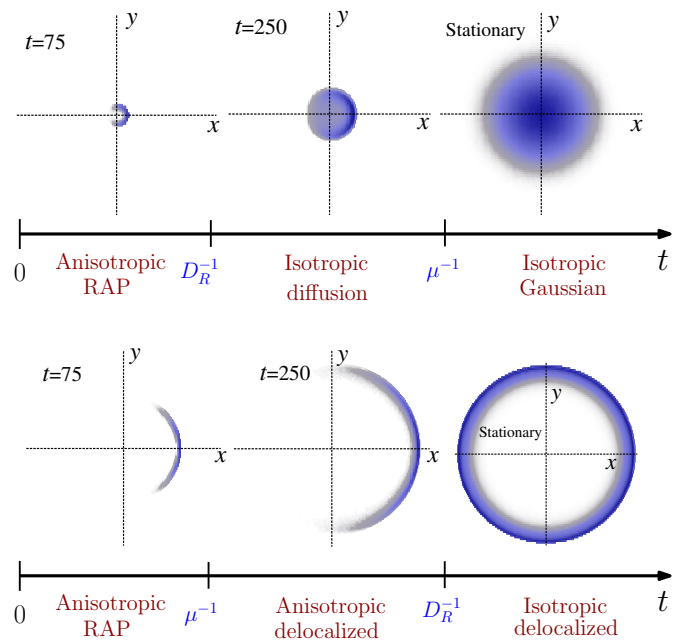


FIG. 6. Position probability distribution $P(x, y, t)$ for an ABP in a 2d harmonic trap of strength μ at different time t . Upper and lower panels correspond to the cases $\mu^{-1} > D_R^{-1}$ and $\mu^{-1} < D_R^{-1}$, respectively. The presence of anisotropy at short-times and the delocalized stationary state (for $\mu^{-1} < D_R^{-1}$) are two specific signatures of activity. The numerical data have been obtained for $D_R^{-1} = 10^2$ and $\mu^{-1} = 10^3$ (upper panel) and $D_R^{-1} = 10^3$ and $\mu^{-1} = 10^2$ (lower panel).

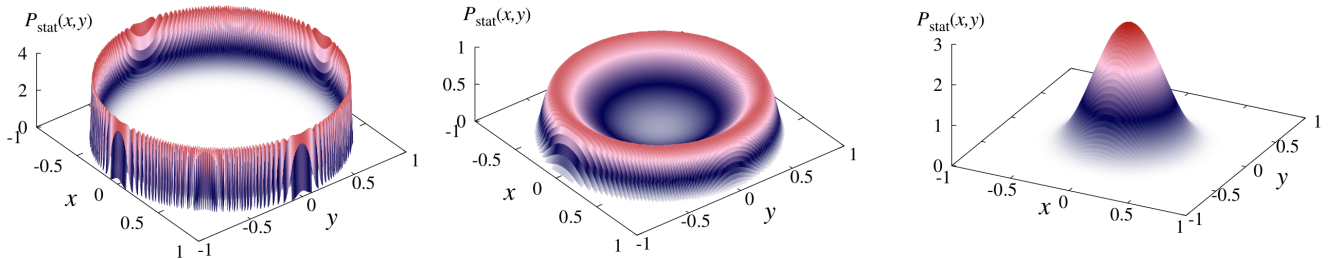


FIG. 7. Stationary distribution $P_{\text{stat}}(x, y)$ of an ABP in a harmonic trap for different values of $D_R = 0.1$ (left), $D_R = 1.0$ (centre) and $D_R = 10.0$ (right). The left and middle panel show the delocalized state where the particle is most likely to be accumulated away from the center. The right panel corresponds to the passive limit where the stationary distribution is Gaussian. Here the trap stiffness $\mu = 1.0$ and $v_0 = 1.0$.

from the full probability density $\mathcal{P}_\mu(x, y, \phi, t)$:

$$P_\mu(x, y, t) = \int d\phi \mathcal{P}_\mu(x, y, \phi, t). \quad (46)$$

Starting from the Langevin equations (45), it is easy to write down the corresponding Fokker-Planck equation,

$$\begin{aligned} \partial_t \mathcal{P}_\mu(x, y, \phi, t) = & \frac{\partial}{\partial x} \left[(\mu x - v_0 \cos \phi) \mathcal{P}_\mu \right] \\ & + \frac{\partial}{\partial y} \left[(\mu y - v_0 \sin \phi) \mathcal{P}_\mu \right] + D_R \frac{\partial^2 \mathcal{P}_\mu}{\partial \phi^2}, \end{aligned} \quad (47)$$

where we have suppressed the argument of \mathcal{P}_μ on the right hand side for brevity.

In the long time limit the position distribution $P_\mu(x, y, t)$ converges to a stationary form which is denoted by

$$P_{\text{stat}}(x, y) = P_\mu(x, y, t \rightarrow \infty). \quad (48)$$

Unfortunately, the Fokker-Planck equation (47) is hard to solve, even for the stationary state. Very recently, in Ref. [41], the same Langevin equation (45) was studied, but in the presence of an additive translational noise in the x and y directions with a nonzero translational diffusion constant D_T . The stationary distribution $P_{\text{stat}}(x, y)$ was computed from the associated Fokker-Planck equation as a power series expansion in terms of the parameter $\lambda = \frac{v_0}{\sqrt{D_R D_T}}$. However, this result cannot be easily extrapolated to the case $D_T = 0$ where $\lambda \rightarrow \infty$ (except in the strongly passive case where $D_R \rightarrow \infty$ limit is taken first). This is because, in general, the two limits do not commute: (i) first $D_T \rightarrow 0$ and then $t \rightarrow \infty$ (ii) first $t \rightarrow \infty$ with finite D_T and then $D_T \rightarrow 0$. While we are interested in limit (i), Ref. [41] studied mostly the limit (ii).

Here we follow a different approach that involves deriving and solving an exact recursion relation satisfied by the moments of the position. A similar method involving recursion of moments was studied by Gredat, Dornic and Luck (GDL) in Ref. [62] in the context of a reaction diffusion equation. In their problem, GDL were interested

in the (imaginary) exponential functional of a Brownian motion with a nonzero drift. Here we adapt their approach to our ABP problem in a harmonic trap. Our recursion relation, though formally appears deceptively similar to that of GDL, the slight difference actually leads to very different physics and results. Indeed in Appendix C we will discuss in detail the differences between the two recursion relations.

It is first convenient to recast the Langevin equations (45) in terms of a complex coordinate $z = x + iy$. Our goal is to evaluate the moment of the type

$$M_{k,l}(t) = \langle z^k(t) \bar{z}^l(t) \rangle, \quad (49)$$

where $\bar{z}(t) = x(t) - iy(t)$ is the complex conjugate of z . From Eq. (45) it immediately follows that $z(t)$ evolves according to,

$$\dot{z} = -\mu z + v_0 e^{i\phi(t)}. \quad (50)$$

which can be formally solved to get,

$$z(t) = v_0 \int_0^t ds e^{-\mu(t-s)} e^{i\phi(s)} \quad (51)$$

We assume that the particle starts initially at the origin $x = y = 0$ with $\phi(0) = 0$. In principle, one can use Eq. (51) and the Gaussian property of the process $\phi(s)$, to express $M_{k,l}(t)$ as a $(k+l)$ -fold multiple integral. However, evaluating this multiple integral explicitly seems very hard. Instead, we will derive below an exact recursion relation for the moments $M_{k,l}(t)$.

To proceed further, it is useful to discretize the continuous time expression of Eq. (51) in a discrete-time setting. We imagine that the interval $[0, t]$ consists of n discrete intervals each of length $\varepsilon > 0$, such that $t = n\varepsilon$. We then split the time interval $[0, t]$ in the integral in Eq. (51) into two separate intervals $[0, \varepsilon]$ and $[\varepsilon, t]$. This gives

$$z(t) = v_0 \left(\int_0^\varepsilon e^{-\mu(t-s)+i\phi(s)} ds + \int_\varepsilon^t e^{-\mu(t-s)+i\phi(s)} ds \right). \quad (52)$$

The first integral, to leading order in ε , gives $e^{-\mu t} \varepsilon$, where we used $\phi(0) = 0$. In the second integral, we

make a change of variable $s = \varepsilon + \tau$ and rewrite it as, $\int_0^{t-\varepsilon} e^{-\mu(t-\varepsilon-\tau)+i\phi(\varepsilon+\tau)} d\tau$. Next we write $\phi(\varepsilon + \tau) = \phi(\varepsilon + \tau) - \phi(\varepsilon) + \phi(\varepsilon)$, i.e., add and subtract $\phi(\varepsilon)$. Putting this together, we get

$$z(t) \approx v_0 \left(e^{-\mu t} \varepsilon + e^{i\phi(\varepsilon)} \int_0^{t-\varepsilon} e^{-\mu(t-\varepsilon-\tau)+i\tilde{\phi}(\tau)} d\tau \right), \quad (53)$$

where

$$\tilde{\phi}(\tau) = \phi(\varepsilon + \tau) - \phi(\varepsilon). \quad (54)$$

Now we will use the crucial property that $\tilde{\phi}(\tau)$ is also a Brownian motion starting at $\tilde{\phi}(0) = 0$, and with correlation function $\langle \tilde{\phi}(t_1) \tilde{\phi}(t_2) \rangle = 2D_R \min(t_1, t_2)$. Importantly, the statistical properties of $\tilde{\phi}(t)$ do not depend on ε . In other words, one can write a statistical identity in law

$$\tilde{\phi}(\tau) \equiv \phi(\tau), \quad (55)$$

where \equiv means that the right hand side and left hand side have identical distributions. Consequently, using this identity (55) and the definition of $z(t)$ in Eq. (51), one gets

$$\int_0^{t-\varepsilon} e^{-\mu(t-\varepsilon-\tau)+i\tilde{\phi}(\tau)} d\tau \equiv z(t-\varepsilon). \quad (56)$$

Hence, (53) provides us with a statistical identity

$$z(t) \equiv v_0 \varepsilon e^{-\mu t} + e^{i\phi(\varepsilon)} z(t-\varepsilon). \quad (57)$$

Denoting $z_n = z(t = n\varepsilon)$ in the discrete-time setting, we then obtain a Kesten type statistical recursion relation

$$z_n \equiv v_0 \varepsilon e^{-\mu n \varepsilon} + \eta_n z_{n-1} \quad (58)$$

where $\eta_n = e^{i\phi(\varepsilon)}$ is an effective noise, independent of z_{n-1} . The complex conjugate \bar{z}_n also satisfies a similar relation,

$$\bar{z}_n = v_0 \varepsilon e^{-\mu n \varepsilon} + \bar{\eta}_n \bar{z}_{n-1}, \quad (59)$$

where $\bar{\eta}_n$ is the complex conjugate of η_n . Using the Gaussian property of $\phi(s)$, one can easily evaluate the moments of the noise η_n . For instance, one gets $\langle \eta_n \rangle = e^{-\varepsilon D_R}$ and correlation $\langle \eta_n^k \bar{\eta}_n^l \rangle = e^{-\varepsilon D_R (k-l)^2}$.

Using Equations (58) and (59) one can now derive a recursion relation for the discrete-time version of the moment $M_{k,l}(n) = \langle z_n^k \bar{z}_n^l \rangle$. We take z_n^k in Eq. (58) and \bar{z}_n^l in Eq. (59), multiply them and then take the expectation value with respect to the noise η_n . We use the independence of η_n and z_{n-1} and the known moments of the noise η_n and then expand in powers of ε . Keeping terms only up to order $O(\varepsilon)$, we get

$$M_{k,l}(n) \simeq [1 - \varepsilon D_R (k-l)^2] M_{k,l}(n-1) + v_0 \varepsilon e^{-\mu n \varepsilon} [k M_{k-1,l}(n-1) + l M_{k,l-1}(n-1)]. \quad (60)$$

Taking the continuous-time limit $\varepsilon \rightarrow 0$ and replacing $(M_{k,l}(n) - M_{k,l}(n-1))/\varepsilon$ by the time derivative $dM_{k,l}/dt$ we arrive at the exact recursion relation

$$\dot{M}_{k,l} = -D_R (k-l)^2 M_{k,l} + v_0 e^{-\mu t} [k M_{k-1,l} + l M_{k,l-1}] \quad (61)$$

with the conditions $M_{0,0}(t) = 1$ at all times and $M_{k,l}(0) = 0$ for $k, l > 0$. We also use the convention $M_{k,l}(t) = 0$ for $k, l < 0$. It is easy to check that $M_{k,l}(t) = M_{l,k}(t)$. Eq. (61) allows us to compute the moments explicitly in a recursive fashion (see Appendix D for the first few values of k, l).

Note that, since the right hand side is explicitly time-dependent, it is not possible to obtain the stationary state by simply equating $\dot{M}_{k,l}$ to zero, rather one has to find the full time-dependent solution and then take long-time limit to find the same. It turns out that this can be done in the two limiting cases, $D_R \rightarrow \infty$ (strongly passive) and $D_R \rightarrow 0$ (strongly active) which are discussed in details below.

Strongly passive limit ($D_R \rightarrow \infty$): To solve the moment evolution Eq. (61) in the limit of $D_R \rightarrow \infty$ we inspect the large D_R behaviour of the first few moments presented in Eq. (D4) in Appendix D. It turns out that these quantities, to the leading order in D_R^{-1} , are of the form,

$$M_{k,l}(t) \simeq \frac{v_0^{k+l} k!}{[(k-l)!]^2} \left[\frac{e^{-\mu t}}{D_R} \right]^k \left[\frac{e^{\mu t} - e^{-\mu t}}{\mu} \right]^l, \quad k \geq l. \quad (62)$$

Indeed, substituting this ansatz in the recursion relation (61), it can be verified that Eq. (61) is indeed satisfied by Eq. (62), up to leading order for large D_R . Note that this leading order result for $M_{k,l}(t)$ in Eq. (62) is actually valid for all time t , including $t = 0$.

To extract further information, we consider the diagonal moments $M_{k,k}(t) = \langle (z(t)\bar{z}(t))^k \rangle$. Using $z(t)\bar{z}(t) = x^2(t) + y^2(t) = r^2(t)$, the diagonal element $M_{k,k}(t) = \langle r^{2k}(t) \rangle$ is precisely the $2k$ -th radial moment of the full distribution. This radial moment is given by,

$$\langle r^{2k}(t) \rangle = \int_0^\infty r^{2k+1} P_{\text{rad}}(r, t) dr. \quad (63)$$

where $P_{\text{rad}}(r, t)$ is the marginal radial distribution,

$$P_{\text{rad}}(r, t) = \int_0^{2\pi} P_\mu(r, \theta, t) d\theta. \quad (64)$$

Here $P_\mu(r, \theta, t)$ denotes the position probability in the radial coordinates, and is equivalent to $P_\mu(x, y, t)$ [63]. Setting $l = k$ in Eq. (62) we then get

$$\langle r^{2k}(t) \rangle = M_{k,k}(t) \simeq \Gamma(k+1) \left[\frac{v_0^2}{\mu D_R} (1 - e^{-2\mu t}) \right]^k. \quad (65)$$

Anticipating a Gaussian behaviour for the radial distribution, we make the ansatz, and check a posteriori, that

$P_{\text{rad}}(r, t)$ has the form $P_{\text{rad}}(r, t) = A(t)e^{-B(t)r^2}$. Substituting this ansatz in Eq. (63) and comparing to the result in (62), we see that

$$A(t) = 2B(t), \quad B(t) = \frac{\mu D_R}{v_0^2(1 - e^{-2\mu t})}. \quad (66)$$

Finally, this gives

$$P_{\text{rad}}(r, t) \simeq \frac{2\mu D_R}{v_0^2(1 - e^{-2\mu t})} \exp\left[-\frac{\mu D_R r^2}{v_0^2(1 - e^{-2\mu t})}\right]. \quad (67)$$

Note that this solution is valid at all times t . In particular, at early times, when $D_R^{-1} \ll t \ll \mu^{-1}$ the solution in Eq. (67) corresponds to free isotropic diffusion with a diffusion constant $D_{\text{eff}} = v_0^2/2D_R$. This scenario corresponds to the upper middle panel in Fig. 6. In contrast, when $t \gg \mu^{-1}$, the radial distribution (67) approaches a stationary form.

Moreover, from Eq. (62) it follows that for $k \neq l$, $M_{k,l}(t)$ decays exponentially with time and vanishes in the long time limit. This indicates that the distribution quickly loses the anisotropy and the stationary distribution becomes radially symmetric. Consequently, the stationary position distribution in Eq. (48) is given by

$$P_{\text{stat}}(x, y) = \frac{1}{2\pi} P_{\text{rad}}(r, t \rightarrow \infty). \quad (68)$$

Using Eq. (67), one gets the expected Boltzmann distribution

$$P_{\text{stat}}(x, y) = \frac{\mu D_R}{\pi v_0^2} \exp\left[-\frac{\mu D_R(x^2 + y^2)}{v_0^2}\right], \quad (69)$$

with an effective temperature $T_{\text{eff}} = v_0^2/2D_R = D_{\text{eff}}$, in full agreement with the experimental observation [31].

Strongly active limit ($D_R = 0$): In this case, the first term on the right hand side of Eq. (61) drops out and it can be checked that

$$M_{k,l}(t) = \left[\frac{v_0}{\mu} (1 - e^{-\mu t})\right]^{k+l} \quad (70)$$

solves the resulting equation at all times t . Again, setting $l = k$ in (70) the time-dependent radial moments are given by

$$\langle r^{2k}(t) \rangle = M_{k,k}(t) = \left[\frac{v_0}{\mu} (1 - e^{-\mu t})\right]^{2k}. \quad (71)$$

Comparing Eq. (63) with Eq. (71) gives the time-dependent marginal radial distribution,

$$P_{\text{rad}}(r, t) = \frac{\mu}{v_0(1 - e^{-\mu t})} \delta\left[r - \frac{v_0(1 - e^{-\mu t})}{\mu}\right]. \quad (72)$$

Note however that strictly for $D_R = 0$, the position distribution $P(x, y, t)$ is not radially symmetric. Indeed, in this case, the Langevin equation (1) in the main text reduces to a pair of deterministic equations:

$$\dot{x} = -\mu x + v_0 \quad \text{and} \quad \dot{y} = -\mu y, \quad (73)$$

with initial conditions $x(0) = y(0) = 0$. Solving these equations give $x(t) = (v_0/\mu)(1 - e^{-\mu t})$ and $y(t) = 0$. Consequently, the position distribution function is given by

$$P_{\mu}(x, y, t) = \delta\left(x - \frac{v_0(1 - e^{-\mu t})}{\mu}\right) \delta(y). \quad (74)$$

One can check that the moment $M_{k,l}(t)$ computed with this distribution is indeed given by (70). Moreover, the radial marginal distribution $P_{\text{rad}}(r, t)$ computed from this two-dimensional distribution is indeed given by (72).

Thus strictly for $D_R = 0$ the position distribution in the $2d$ -plane is highly anisotropic. This is true even in the $t \rightarrow \infty$ limit, where we see from Eq. (70) that

$$M_{k,l}(t \rightarrow \infty) = \left(\frac{v_0}{\mu}\right)^{k+l} \quad \text{for all } k, l. \quad (75)$$

Thus, the off-diagonal elements remain non-zero as $t \rightarrow \infty$, indicating the presence of anisotropy in the stationary state.

However, for any finite $D_R > 0$, the rotational diffusion spreads the particle position uniformly over the angle $[0, 2\pi]$. Consequently, in the long time limit and $D_R \rightarrow 0^+$, the position distribution approaches a stationary form that is fully isotropic in the $2d$ plane. Indeed, from the exact expression for the moments in (D4), it is easy to verify that, for $D_R \rightarrow 0^+$, the off-diagonal elements decay as $M_{k,l}(t) \sim e^{-D_R(k-l)^2 t}$ at late times, for $k \neq l$. In particular, for $t \gg D_R^{-1}$, $M_{k,l}(t) \rightarrow 0$ for $k \neq l$. In contrast, the diagonal elements approach to non-zero values as $t \rightarrow \infty$. More precisely, we find

$$M_{k,k}(t \rightarrow \infty) \rightarrow \left(\frac{v_0}{\mu}\right)^{2k} \\ M_{k,l}(t \rightarrow \infty) \rightarrow 0, \quad k \neq l. \quad (76)$$

Note the difference with the strictly $D_R = 0$ case in Eq. (75). Consequently, in this $D_R \rightarrow 0^+$ limit, for $t \gg D_R^{-1}$, it follows from Eq. (76) that the position distribution approaches an isotropic form in the stationary limit and is given by

$$P_{\text{stat}}(x, y) = \frac{\mu}{2\pi v_0} \delta\left[\sqrt{x^2 + y^2} - \frac{v_0}{\mu}\right] \quad (77)$$

where the particle is strongly confined at the boundary of the trap $r_b = v_0/\mu$. This non-Boltzmann distribution results from the strongly active nature of the dynamics.

Figure 7 shows the stationary distribution $P_{\text{stat}}(x, y)$ in the (x, y) plane obtained from simulations, for different D_R . As D_R decreases, the stationary distribution shows a crossover from the passive regime, with a single-peaked Gaussian around $r = 0$, to the active regime, with a delocalized state where the particle is confined around a narrow ring away from the origin, at $r_b = v_0/\mu$.

V. CONCLUSION

To summarize, this paper has two parts. In the first part, we have studied the late time dynamics of a free ABP in two dimensions, focussing on the position distribution $P(x, y, t)$. We have showed that while the typical fluctuations are described by a Gaussian distribution as expected from the central limit theorem, large fluctuations, where $\sqrt{x^2 + y^2} \sim \mathcal{O}(v_0 t)$, are described by non-Gaussian tails. These rare fluctuations capture the signature of ‘activity’ even at late times t . In this regime we have showed that $P(x, y, t)$ admits a large deviation form $P(x, y, t) \sim \exp[-D_R t \Phi(z)]$ where $z = \sqrt{x^2 + y^2}/(v_0 t)$. We have computed the rate function $\Phi(z)$ both analytically and numerically.

Another way to observe the fingerprints of activity in the position distribution at late times is to switch on an external harmonic potential with stiffness μ . In this case the position distribution approaches a stationary form at late times and the stationary distribution $P_{\text{stat}}(x, y)$ depends explicitly on the activity parameter D_R^{-1} . We compute the stationary distribution explicitly in the two opposite limits: (i) strongly active ($D_R \rightarrow 0$) and (ii) strongly passive ($D_R \rightarrow \infty$). In the former case the distribution is ring shaped with ring radius $r = v_0/\mu$, while in the latter case it is a Gaussian centered at the origin. As D_R increases the shape of the distribution smoothly crosses over from the ring shape to the Gaussian shape. This is in agreement with the results seen in experiments [31] and simulations [23, 27].

We find it remarkable that even for this simplest ABP model (free or harmonically confined) the position distribution $P(x, y, t)$ cannot be computed exactly at all times in the real space. At least in this paper we managed to compute analytically the large deviation function that describes the atypical fluctuations at late times for the free ABP. Of course there are many interesting open questions related to our work. For example, it would be interesting to study the dynamics of an ABP in higher dimensions and derive the associated rate function $\Phi(z)$. In this paper we have focused on a single ABP—it would be interesting to derive the large deviation function associated with the late time density profile of a gas of *interacting* ABP’s. Finally, in the presence of a confining potential, we have studied the stationary state in the case of an isotropic harmonic trap. It would be interesting to study the position distribution of an ABP in an anisotropic harmonic trap, or more generally for anharmonic traps, in two or higher dimensions.

ACKNOWLEDGMENTS

We thank I. Dornic and J. M. Luck for useful discussions and for pointing out the Ref. [47] to us. We acknowledge support from the project 5604-2 of the Indo-French Centre for the Promotion of Advanced Research (IFCPAR). SNM acknowledges the support from the Sci-

ence and Engineering Research Board (SERB, government of India) under the VAJRA faculty scheme (Ref. VJR/2017/000110) during a visit to the Raman Research Institute in 2019, where part of this work was carried out. U.B. acknowledges support from Science and Engineering Research Board (SERB), India under Ramanujan Fellowship (Grant No. SB/S2/RJN-077/2018).

Appendix A: Exact solution of Mathieu Eigenfunctions

As explained in Section III, we are interested only in the π -periodic even solutions of the Mathieu equation

$$ce_{2n}''(v, q) + (a_{2n}(q) - 2q \cos 2v)ce_{2n}(v, q) = 0 \quad (\text{A1})$$

where $a_{2n}(q)$ are the associated eigenvalues. To calculate the moments and the large deviation function we only need the lowest eigenvalue. The series expansion of that lowest eigenvalue $a_0(q)$ is known for both in the small q and large q limit. For small q ,

$$a_0(q) = \sum_{n=1}^{\infty} \alpha_{2n} q^{2n}. \quad (\text{A2})$$

The first few coefficients are quoted here,

$$\begin{aligned} \alpha_2 &= -\frac{1}{2}, & \alpha_4 &= \frac{7}{128}, \\ \alpha_6 &= -\frac{1}{2304}, & \alpha_8 &= \frac{68687}{18874368}, \dots \end{aligned} \quad (\text{A3})$$

On the other hand, in the large q limit, the expansion is given by,

$$a_0(q) = \sum_{n=0}^{\infty} \beta_n q^{1-\frac{n}{2}} \quad (\text{A4})$$

where

$$\begin{aligned} \beta_0 &= -2, & \beta_1 &= 2, & \beta_2 &= -\frac{1}{4}, \\ \beta_3 &= -\frac{1}{32}, & \beta_4 &= -\frac{3}{256}, & \beta_5 &= -\frac{53}{8192} \dots \end{aligned} \quad (\text{A5})$$

Appendix B: Systematic determination of $\Phi(z)$

Equation (12) in the main text relates the large deviation function $\Phi(z)$ to the eigenvalue a_0 through a Legendre transform,

$$\min_{-1 \leq z \leq 1} \left[\frac{p}{D_R} z + \Phi(z) \right] = \frac{1}{4} a_0 \left(\frac{2p}{D_R} \right) \quad (\text{B1})$$

The large deviation function can be extracted from the inverse transform,

$$\Phi(z) = \max_{h \in \mathbb{R}} \left[\frac{1}{4} a_0(2h) - hz \right] \quad (\text{B2})$$

where we have defined $h = p/D_R$. The large deviation function is then given by,

$$\Phi(z) = \frac{1}{4}a_0(2h^*(z)) - zh^*(z) \quad (\text{B3})$$

where $h^*(z)$ is the value of h corresponding to the maximum of the function $g_z(h) = \frac{1}{4}a_0(2h) - zh$, and can be obtained by setting its derivative to zero, *i.e.*, by solving

$$\frac{1}{4} \frac{d}{dh} a_0(2h) = z. \quad (\text{B4})$$

As $a_0(2h)$ is known as the sum of an infinite series in h (see Eqs. (A2)-(A4)), it is best to solve the above equation recursively. It is easy to see that for small values of z , h^* is also small while for $z \rightarrow \pm 1$, the maximum occurs at large values of h^* [64]. It is then convenient to use Eq. (A2) (respectively Eq. (A4)) for finding $h^*(z)$ near $z = 0$ (respectively near $z = \pm 1$).

Let us first look at the case $z \approx 0$. In this case, using the series (A2), Eq. (B4) becomes,

$$\frac{1}{2} \sum_{n=1}^{\infty} \alpha_{2n} n 2^{2n} (h^*)^{2n-1} = z \quad (\text{B5})$$

In the following we solve this equation recursively to systematically determine $\Phi(z)$ as a series in z . To the lowest order, *i.e.*, keeping the term linear in h only, we have,

$$2\alpha_2 h^* = z, \quad (\text{B6})$$

which, using the value of α_2 (see Eq. (A3)) yields $h^* = -z$. This value of h^* , substituted in Eq. (B3), and keeping the lowest order term again, gives,

$$\Phi(z) \approx \frac{1}{2} z^2. \quad (\text{B7})$$

Equation (B7) implies that, close to the origin $z = 0$, in the long time limit, the position distribution is Gaussian. The higher order corrections can also be systematically calculated in a recursive manner.

Since both $\Phi(z)$ and $a_0(2h)$ are even functions of their arguments, it is easy to see that h^* must be an odd function of z , and we can write a series expansion,

$$h^*(z) = \sum_{m=1,3,\dots}^{\infty} c_m z^m. \quad (\text{B8})$$

Substituting this form in Eq. (B5), and then comparing coefficients of powers of z on both sides, one can solve for the c_m recursively. Clearly, $c_1 = -1$, as we have explicitly shown above. The next few coefficients are computed using Mathematica and are quoted below,

$$c_3 = -\frac{7}{8}, c_5 = -\frac{209}{192}, c_7 = -\frac{53231}{294912} \quad (\text{B9})$$

Using these coefficients, and substituting Eq. (B8) in Eq. (B3) one can construct $\Phi(z)$ as a series expansion in z , which is given in Eq. (14) in the main text.

The behaviour of $\Phi(z)$ near the boundaries $z = \pm 1$ can also be extracted in a similar manner. As $\Phi(z)$ is an even function of z , it suffices to compute it near one boundary, say $z = -1$. We follow the same procedure as traced above, but use Eq. (A4) for a_0 . Accordingly, Eq. (B5) becomes,

$$\sum_{n=0}^{\infty} \frac{\beta_n}{2^{1+\frac{n}{2}}} \left(1 - \frac{n}{2}\right) (h^*)^{-\frac{n}{2}} = z \quad (\text{B10})$$

which we solve order by order to find $h^*(z)$.

To the lowest order, we have,

$$\beta_0 + \frac{\beta_1}{2^{3/2}\sqrt{h^*}} = 2z \quad (\text{B11})$$

which, after substituting the values of β_0 and β_1 , yields, $h^* = 1/8(1+z)^2$. Using this value of h^* in Eq. (B3), we get, near $z = -1$,

$$\Phi(z) \approx \frac{1}{8(1+z)}. \quad (\text{B12})$$

The higher order corrections are systematically obtained by assuming a series expansion for h^* ,

$$h^*(z) = \sum_{n=-2}^{\infty} b_n (1+z)^n \quad (\text{B13})$$

where $b_{-2} = 1/8$, as shown above. The coefficients b_n for $n > -2$ can be obtained by substituting Eq. (B13) in Eq. (B11) and equating coefficients of powers of $1+z$ on both sides. This exercise gives,

$$b_{-1} = 0, b_0 = \frac{1}{64}, b_1 = \frac{3}{128}. \quad (\text{B14})$$

The large deviation function $\Phi(z)$ near $z = -1$ is then obtained using Eq. (B13) in Eq. (B3), and is given by,

$$\Phi(z) = \frac{1}{8(1+z)} - \frac{1}{16} - \frac{(1+z)}{64} - \frac{3}{256}(1+z)^2 - \frac{51}{4096}(1+z)^3 + \dots \quad (\text{B15})$$

Using the symmetry of $\Phi(z)$, its behaviour near $z = 1$ can be obtained from the above equation by substituting $z \rightarrow -z$. This is quoted in the main text in the second line of Eq. (14).

Appendix C: Connection to GDL

In Ref. [62] Gredat, Dornic, Luck (GDL) were interested in the imaginary exponential functional of a Brownian motion and studied an effective process given by

$$z^{GDL}(t) = v_0 \int_0^t e^{-\mu s + i\phi(s)} ds. \quad (\text{C1})$$

The two processes, $z(t)$ in (51) and $z^{GDL}(t)$ in (C1), look deceptively similar. However it turns out that they

have rather different properties and in fact the recursion relation for the moments turn out to be rather different.

A recursion relation for the discretized version of $z^{GDL}(t)$ can be derived following scheme similar to the one used for $z(t)$ in the main text, and yields [62],

$$z_n^{GDL} \equiv v_0 \varepsilon + e^{-\mu \varepsilon} \eta_n z_{n-1}^{GDL}, \quad (C2)$$

which is manifestly different from our recursion relation (58).

Correspondingly, the recursion relation for the moments $\tilde{M}_{k,l}(t) = M_{k,l}^{GDL}(t)$ in the GDL case also turns out to be very different [62],

$$\begin{aligned} \frac{d}{dt} \tilde{M}_{k,l} = & -(\mu(k+l) + D_R(k-l)^2) \tilde{M}_{k,l} \\ & + v_0 (k \tilde{M}_{k-1,l} + l \tilde{M}_{k,l-1}). \end{aligned} \quad (C3)$$

Note that there is no explicit time dependence on the right hand side of this equation (C2) and the moments in the stationary state can be simply obtained by setting the time derivative to be zero on the left hand side of (C2). As mentioned above, the situation in our case is completely different.

Appendix D: Solution of the moment recursion relation

The moments $M_{k,l}(t)$ evolve according to,

$$\dot{M}_{k,l} = -D_R(k-l)^2 M_{k,l} + v_0 e^{-\mu t} [k M_{k-1,l} + l M_{k,l-1}]$$

$$\begin{aligned} M_{1,0}(t) &= \frac{v_0(e^{-\mu t} - e^{-D_R t})}{D_R - \mu} \\ M_{1,1}(t) &= \frac{v_0^2}{(D_R - \mu)} \left[\frac{1 - e^{-2\mu t}}{\mu} - \frac{2(1 - e^{-(D_R + \mu)t})}{D_R + \mu} \right] \\ M_{2,0}(t) &= \frac{v_0^2[(3D_R - \mu)e^{-2\mu t} - 2(2D_R - \mu)e^{-(D_R + \mu)t} + (D_R - \mu)e^{-4D_R t}]}{(D_R - \mu)(2D_R - \mu)(3D_R - \mu)}. \end{aligned} \quad (D4)$$

As we see, the solutions quickly become long and cumbersome as k and l increase. Fortunately, Eq. (D1) can

$$M_{k,l}(t) = M_{l,k}(t). \quad (D1)$$

We can think of (k, l) as the grid points on the $2d$ lattice with $k, l \geq 0$. We note that by definition $M_{0,0}(t) = 1$ at all times t . As a result, it is easy to see from the recursion relation (D1) that the solution $M_{k,l}(t)$ is symmetric under exchange of k and l , *i.e.*,

$$M_{k,l}(t) = M_{l,k}(t). \quad (D2)$$

Hence, it is sufficient to study $M_{k,l}(t)$ only for $k \geq l$. The recursion relations for the first few values of k and l read, for instance (with the convention that $M_{k,l}(t) = 0$ for $k, l < 0$)

$$\begin{aligned} \dot{M}_{1,0}(t) &= -D_R M_{1,0}(t) + v_0 e^{-\mu t} M_{0,0}(t) \\ \dot{M}_{1,1}(t) &= 2v_0 e^{-\mu t} M_{1,0}(t) \\ \dot{M}_{2,0}(t) &= -4D_R M_{2,0}(t) + 2v_0 e^{-\mu t} M_{1,0}(t) \end{aligned} \quad (D3)$$

and so on. These equations can be solved recursively, *i.e.*, using the solution of the previous equation. The solution of these first few moments can be written explicitly at all times t ,

be solved exactly to find $M_{k,l}(t)$ for all k and l in the two limiting cases ($D_R \rightarrow \infty$ and $D_R = 0$) which is done in the main text.

-
- [1] P. Romanczuk, M. Bär, W. Ebeling, B. Lindner, and L. Schimansky-Geier, Eur. Phys. J. Special Topics **202**, 1 (2012).
 [2] M. C. Marchetti, J. F. Joanny, S. Ramaswamy, T. B. Liverpool, J. Prost, M. Rao, and R. Aditi Simha, Rev. Mod. Phys. **85**, 1143 (2013).
 [3] C. Bechinger, R. Di Leonardo, H. Löwen, C. Reichhardt, G. Volpe, and G. Volpe, Rev. Mod. Phys. **88**, 045006

- (2016).
 [4] S. Ramaswamy, J. Stat. Mech. 054002 (2017).
 [5] É. Fodor, and M. C. Marchetti, Physica A **504**, 106 (2018).
 [6] *E. Coli in Motion*, H. C. Berg, (Springer Verlag, Heidelberg, Germany) (2004).
 [7] M. E. Cates, Rep. Prog. Phys. **75**, 042601 (2012).

- [8] X. Trepát, M. R. Wasserman, T. E. Angelini, E. Millet, D. A. Weitz, J. P. Butler, and J. J. Fredberg, *Nature Physics* **5**, 426 (2009).
- [9] T. Vicsek, A. Czirók, E. Ben-Jacob, I. Cohen, and O. Shochet, *Phys. Rev. Lett.* **75**, 1226 (1995).
- [10] S. Hubbard, P. Babak, S. Th. Sigurdsson, and K. G. Magnússon, *Ecological Modelling*, **174**, 359 (2004).
- [11] D. L. Blair, T. Neicu, and A. Kudrolli, *Phys. Rev. E* **67**, 031303 (2003).
- [12] L. Walsh, C. G. Wagner, S. Schlossberg, C. Olson, A. Baskaran, and N. Menon, *Soft Matter* **13**, 8964 (2017).
- [13] J. Palacci, S. Sacanna, A. P. Steinberg, D. J. Pine, and P. M. Chaikin, *Science* **339**, 936 (2013).
- [14] J. Toner, Y. Tu, and S. Ramaswamy, *Ann. of Phys.* **318**, 170 (2005).
- [15] N. Kumar, H. Soni, S. Ramaswamy, and A. K. Sood, *Nature Comm.* **5**, 4688 (2014).
- [16] Y. Fily, and M. C. Marchetti, *Phys. Rev. Lett.* **108**, 235702 (2012).
- [17] A. B. Slowman, M. R. Evans, R. A. Blythe, *Phys. Rev. Lett.* **116**, 218101 (2016).
- [18] A. B. Slowman, M. R. Evans, R. A. Blythe, *J. Phys. A: Math. Theor.* **50**, 375601 (2017).
- [19] J. Schwarz-Linek, C. Valeriani, A. Cacciuto, M. E. Cates, D. Marenduzzo, A. N. Morozov, and W. C. K. Poon, *Proc. Natl. Acad. Sci. USA* **109**, 4052 (2012).
- [20] G. S. Redner, M. F. Hagan, and A. Baskaran, *Phys. Rev. Lett.* **110**, 055701 (2013).
- [21] J. Stenhammar, R. Wittkowski, D. Marenduzzo, and M. E. Cates, *Phys. Rev. Lett.* **114**, 018301 (2015).
- [22] A. P. Solon, Y. Fily, A. Baskaran, M. E. Cates, Y. Kafri, M. Kardar, and J. Tailleur, *Nature Physics* **11**, 673 (2015).
- [23] A. Pototsky, and H. Stark, *Europhys. Lett.* **98**, 50004 (2012).
- [24] K. Martens, L. Angelani, R. Di Leonardo, and L. Bocquet, *Eur. Phys. J. E* **35**, 84 (2012).
- [25] L. Angelani, R. Di Leonardo, and M. Paoluzzi, *Euro. J. Phys. E* **37**, 59 (2014).
- [26] F. J. Sevilla, and L. A. Gómez Nava, *Phys. Rev. E* **90**, 022130 (2014).
- [27] A. P. Solon, M. E. Cates, and J. Tailleur, *Eur. Phys. J. Special Topics* **224**, 1231 (2015).
- [28] J. Elgeti and G. Gompper, *Europhys. Lett.* **109** 58003 (2015).
- [29] L. Angelani, *J. Phys. A: Math. Theor.* **48** 495003 (2015).
- [30] P. Pietzonka, K. Kleinbeck, and U. Seifert, *New J. Phys.* **18**, 052001 (2016).
- [31] S. C. Takatori, R. De Dier, J. Vermant, and J. F. Brady, *Nature Comm.* **7**, 10694 (2016).
- [32] L. Angelani, *J. Phys. A: Math. Theor.* **50** 325601 (2017).
- [33] K. Malakar, V. Jemseena, A. Kundu, K. Vijay Kumar, S. Sabhapandit, S. N. Majumdar, S. Redner, A. Dhar, *J. Stat. Mech.* 043215 (2018).
- [34] T. Demaerel and C. Maes, *Phys. Rev. E* **97**, 032604 (2018).
- [35] U. Basu, S. N. Majumdar, A. Rosso, G. Schehr, *Phys. Rev. E* **98**, 062121 (2018).
- [36] C. Kurzthaler, C. Devailly, J. Arlt, T. Franosch, W. C. K. Poon, V. A. Martinez, and A. T. Brown, *Phys. Rev. Lett.* **121**, 078001 (2018).
- [37] T. GrandPre, and D. T. Limmer, *Phys. Rev. E* **98**, 060601(R) (2018).
- [38] M. R. Evans and S. N. Majumdar, *J. Phys. A: Math. Theor.* **51**, 475003 (2018).
- [39] A. Dhar, A. Kundu, S. N. Majumdar, S. Sabhapandit and G. Schehr, *Phys. Rev. E*, **99**, 032132 (2019).
- [40] G. Gradenigo and S. N. Majumdar, *J. Stat. Mech.* 053206 (2019).
- [41] K. Malakar, A. Das, A. Kundu, K. Vijay Kumar, A. Dhar, *arXiv:1902.04171*
- [42] O. Dauchot, V. Démery, *Phys. Rev. Lett.* **122**, 068002 (2019).
- [43] P. Le Doussal, S. N. Majumdar, and G. Schehr, *Phys. Rev. E* **100**, 012113 (2019).
- [44] P. Singh and A. Kundu, *J. Stat. Mech.* 083205 (2019).
- [45] F. J. Sevilla, A. V. Arzola, and E. P. Cital, *Phys. Rev. E* **99**, 012145 (2019).
- [46] L. Caprini, E. Hernández-García, C. López, and U. M. B. Marconi, preprint arXiv:1906.03016.
- [47] D. Mumford, *Elastica and Computer Vision*, in Algebraic Geometry and its Applications, edited by C. L. Bajaj, Springer, New York (1994)
- [48] S. N. Majumdar, *Curr. Sci.* **77**, 370 (1999).
- [49] M. Abramowitz and I. A. Stegun (Eds.). *Handbook of Mathematical Functions with Formulas, Graphs, and Mathematical Tables*, 9th printing. New York: Dover, p. 928, 1972.
- [50] J. L. Lebowitz, and H. Spohn, *J. Stat. Phys.* **95**, 333 (1999).
- [51] A. K. Hartmann, *Phys. Rev. E* **65**, 056102 (2002).
- [52] A. K. Hartmann, *Eur. Phys. J. B* **84**, 627 (2011).
- [53] C. Nadal, S. N. Majumdar and M. Vergassola, *J. Stat. Phys.*, **142**, 403 (2011).
- [54] S. N. Majumdar, C. Nadal, A. Scardicchio, and P. Vivo, *Phys. Rev. E*, **83**, 041105 (2011).
- [55] G. Claussen, A. K. Hartmann, and S. N. Majumdar, *Phys. Rev. E*, **91**, 052104 (2015).
- [56] T. Dewenter, G. Claussen, A. K. Hartmann, and S. N. Majumdar, *Phys. Rev. E*, **94**, 052120 (2016).
- [57] H. Schawe, A. K. Hartmann, S. N. Majumdar, *Phys. Rev. E* **96**, 062101 (2017).
- [58] H. Schawe, A. K. Hartmann, S. N. Majumdar, *Phys. Rev. E* **97**, 062159 (2018).
- [59] H. Schawe and A. K. Hartmann, *Eur. Phys. J. B* **92**, 73 (2019).
- [60] A. K. Hartmann, P. Le Doussal, S. N. Majumdar, A. Rosso, G. Schehr, *Europhys. Lett.* **121**, 67004 (2018).
- [61] J. Borjes, H. Schawe, and A. K. Hartmann, *Phys. Rev. E* **99**, 042104 (2019).
- [62] D. Gredat, I. Dornic, and J. M. Luck, *J. Phys. A: Math. Theor.* **44**, 175003 (2011).
- [63] Note that, in polar coordinates, the normalization of the total probability translates to $\int_0^\infty r P_{\text{rad}}(r, t) dr = 1$.
- [64] To be convinced one can simply plot $g_z(h)$ for different values of z .